Hydrogenic impurity effect on optical properties of Wannier-Mott exciton confined in a spherical quantum dot with Kratzer potential under magnetic field

Varsha

Department of Physics and Astrophysics, University of Delhi, Delhi-110007, India,
Department of Physics, Kalindi College, University of Delhi, Delhi-110008, India,
e-mail: varsha.yadav610@gmail.com

R. Giri

Department of Physics and Electronics, Rajdhani College, University of Delhi, Delhi-110015, India.
e-mail: rgirirc@gmail.com

M. Arora

Department of Mathematics, Miranda House, University of Delhi, Delhi-110007, India.
e-mail: monikaaroramh@gmail.com

V. Prasad*

Department of Physics, Swami Shraddhanand College, University of Delhi, Delhi-110036, India.
e-mail: vprasad@ss.du.ac.in

Received 25 March 2022; accepted 13 April 2022

Confinement effects of Kratzer potential on a Wannier-Mott Exciton(W-M) are studied in a spherical quantum dot(QD) in the presence of a static magnetic field. Time independent Schrödinger equation is solved numerically to obtain the energy states. The excitonic transitions so realized have been used to explore the non-linear optical properties that are important for optical characterization of materials such as the optical absorption coefficients (ACs) and refractive index changes (RICs). Impact of magnetic field, strength of the laser field and transition parameters using familiar compact density matrix approach are also analyzed. It has been observed that optical properties get radically modified under confinement effects. Also, the shift of degeneracy of different excitonic energy levels with the magnetic field in confinement potential has been reported for the first time for W-M exciton in the spherical quantum dot, the study that may have crucial input to the literature and myriad of practical implications.

Keywords: Wannier-Mott exciton; quantum dot; magnetic field; linear and non-linear optical absorption coefficients; refractive index changes.

DOI: https://doi.org/10.31349/RevMexFis.68.050504

1. Introduction

Nanomaterials grabbed the most attention of the researchers due to their completely different properties from bulk materials. A lot of deliberate research is going on currently due to promising applications of nanomaterials in diverse fields. The reason for this inclination is owing to the fact that as we go in low dimensions as in QDs , without loss of generality, we get single discrete levels instead of the band structure, and hence become the greatest promising nanomaterials for wide variety of electronic applications like solar cells, transistors, LEDs, medical imaging, quantum computing, and hence have been explored both theoretically and experimentally [1-7]. QDs properties lie in between bulk semiconductors and discrete atoms/molecules. QDs can have different shapes and sizes and rapid progress has been made in fabrication techniques of various QDs. We can have spherical, semi-spherical, disk, ring, or elliptical shapes[8-11]. The size of the quantum dot is very crucial in the measurement of energies of the system. Large size QDs emission spectra lie in the red wavelength region and small size QDs in the blue region.

Analog to electron-proton bound systems in solid-state physics, in semiconductor nanomaterials, we have electron and hole pairs whose bound state is called an exciton, which is the result of Coulomb interaction. Between confined electron and hole, the study of exciton in QD breeds a new arena of application as shown by various researchers in earlier studies [20].

For semiconductors, we have a high susceptibility value, which implies less binding energy, so it is fair to consider Wannier-Mott(W-M) exciton with a large radius due to screening of Coulomb force between electron-hole pair. The W-M model- [12] has three assumptions i) Parabolic bands are used instead of real band structure ii)Valance and conduction bands wave function's minute shape is spurned and iii) In real space, localization of dielectric function is considered.

Experimentalists successfully observed exciton in QDs in different materials [13-15], the results of which have been verified by theoreticians as well. QDs have spectacular optical and electronic properties and hence their study is significant in designing optoelectronic devices. Various factors af-

fecting the optical properties like the electric field, magnetic field, impurity factor, different confining potential, temperature, and hydrostatic pressure etc. [16-19] have been studied extensively.

QDs demonstrate enhanced response to the external fields and hence show varied non-linear optical properties such as absorption coefficients(ACs) and refractive index changes(RICs). These materials can be used in tunable QD laser [21] as the energy of excitonic states changes due to confinement.

Excitonic interactions have been studied in numerous confining potentials like quantum ring [22], parabolic confinement [23-25], Gaussian confinement [26] etc. In the present paper, we have studied non-linear optical properties in a Kratzer potential in a spherical QD under the effect of periodic laser field and magnetic field. Kratzer potential is very near to realistic experimental potential and has applications in atomic and molecular physics [27], quantum chemistry [28], information theory [29], nuclear physics [25-30]. It is a very elementary interaction potential model in quantum mechanics, a special case of the general form of Lennard-Jones potential and closely resembles the Morse potential [31,32]. The novel properties of QDs arise from shape of confining potential as it precisely affects the energy and behavior of exciton in the laser field.

Due to the importance of Kratzer potential, low-dimensional studies have captured a lot of attention [33,34] of many researchers. Batra and Prasad [35] have studied the optical properties of conduction band electrons of spherical QD in Kratzer potential, in the work, they have shown that not only parameters of the QD but also the parameters of Kratzer potential influence optical properties quite drastically. Non-central Kratzer potential also is now highly pursued potential in two dimensional and three-dimensional quantum systems [36]. In a recent paper, we have shown results of the energy of the W-M exciton in spherical QD in Kratzer potential and its dependence on the size of QD, potential parameter, and permittivity of the medium [38]. So far, electronic properties have been studied mostly using this potential [37]. However, in this work, we extend our study to excitonic transitions, as in low dimensional systems, excitons play an imperative role in understanding the basic physics of the system. Compared to Refs. [35,37], here we have considered excitonic transitions in external magnetic field with Kratzer potential confinement and optical response is studied using laser pulse. The screened Coulomb interaction plays a significant role in this study as the dielectric constant of the medium introduces the screening of the above-said force. Many researchers have solved Schrödinger equation of system using variational [40,41], the Nikiforov-Uvarov [42] or the asymptotic iteration method [43]. Due to the trivial behavior of the system, we have solved the Schrödinger equation using the finite difference method (FDM) along with perturbation theory [39]. The advantage of the FDM is that it gives quick accurate results, is low on memory and is more efficient for the evaluation of eigenstates of complex nanostructures with particular shapes. Silotia, Joshi and Prasad [44] studied the energy spectrum and dipole matrix(DM) for a multiple quantum well in the static magnetic field and intense laser pulse using finite difference method. Nautiyal and Silotia [45] studied the second harmonic generation in a disk-shaped QD in the presence of spin-orbit interaction within the framework of FDM.

Further, we have calculated the optical ACs and RICs for W-M exciton in a spherical QD in the magnetic field with and without Kratzer potential and studied the pattern of change in optical properties(ACs and RICs) in the presence of magnetic field using compact density matrix approach that has been well documented in the available literature. Present work is the extension of our previous work where we calculated the ACs and RICs both linear and third-order non-linear without the strength of the magnetic field and in the present manuscript, we are calculation ACs and RICs with magnetic field presence for different excitonic transitions, which may be helpful for the understanding of favorable transitions for better optical response to external fields in the future studies and device designing.

The paper has been organized as follows: Section 2 gives the theoretical understanding essential for this problem, Sec. 3 gives the details of the results and discussion so obtained and Sec. 4 illustrates the brief conclusion of the findings of this paper.

2. Theoretical mathod

We consider a Wannier-Mott exciton confined in a 3D spherical quantum dot with confinement potential defined by $V_c(r)$. Using normal mathematical calculations for the centre of mass and relative motion of the exciton can be separated out and as is well known that the dynamics of the system is understood by considering only the relative part of the Hamiltonian. For further presentation, we only present results and equation related to the relative motion of the system. The relative part of the Hamiltonian for the excitonic system in the absence of magnetic field using effective mass approximation is(for details please see [9, 20])

$$H_0 = \frac{p^2}{2\mu} + V_c(r) - \frac{e^2}{\epsilon r} \tag{1}$$

where H_0 denotes the unperturbed Hamiltonian, $\vec{p}$ is the momentum of the W-M exciton, μ is the reduced mass of exciton given by $\mu = (m_e^* m_h*)/(m_e^* + m_h*)$ where m_e^* is the effective mass of the electron and m_h^* is the effective mass of the hole, ϵ is the permittivity of the medium in which exciton is embedded, e is the charge of electron, r is the separation between electron and hole.

The total confining potential, $V_c(r) = V_1(r) + V_2(r)$, where $V_1(r)$ represents hard spherical confinement potential and is given by:

$$V_1(r) = \begin{cases} 0, & |\mathbf{r}| < \mathbf{R} \\ \infty, & |\mathbf{r}| \geq \mathbf{R}. \end{cases} ,$$

where R is the radius of the QD and $V_2(r)$ is having the form of Kratzer potential which will be defined later on.

From the expression of $V_1(r)$, it is clear that this confinement squeezes the excitons and creates a quantum confining region which is identical to a particle confined in a box. $V_2(r)$ is the potential available inside the QD. Next, we apply a magnetic field in the z-direction, then the interaction Hamiltonian is given by,

$$H = \frac{(\vec{p} + \frac{e}{c}\vec{A})^2}{2\mu} + V_2(r) - \frac{e^2}{\epsilon r}. \quad (2)$$

Magnetic field introduces the Zeeman Splitting between the excitonic energy levels.

$\vec{A}$ is the vector potential written as

$$\vec{A} = \left(-\frac{1}{2}\ (\vec{r} \times \vec{B})\right), \quad (3)$$

Using spherical polar coordinates *i.e.*

$$x = r\sin\theta\cos\phi, \quad y = r\sin\theta\sin\phi, \quad z = r\cos\theta, \quad (4)$$

we get the Hamiltonian as:

$$H = \frac{p^2}{2\mu} + \frac{e^2B^2r^2\sin^2(\theta)}{8\mu c^2} + \frac{eBL_z}{2\mu c} + V_2(r) - \frac{e^2}{\epsilon r}. \quad (5)$$

Here, the magnetic field dependent term is treated as a perturbation as it's magnitude is small compared to the other terms. Hence, the total Hamiltonian can be rearranged into two terms as

$$H = H_0 + H_1, \quad (6)$$

where, H_0 is the unperturbed Hamiltonian given by Eq. (1) and H_1 is the perturbed Hamiltonian given as:

$$H_1 = \frac{e^2B^2r^2\sin^2(\theta)}{8\mu c^2} + \frac{eBL_z}{2\mu c}. \quad (7)$$

Our first task is to find the excitonic levels for unperturbed Hamiltonian H_0 satisfying the following equation $H_0\ \psi_{nlm} = E_{nlm}\ \psi_{nlm}$ inside the QD. Here ψ_{nlm} are unperturbed wavefunctions and E_{nlm} are unperturbed energies.

Using spherical polar coordinates and applying method of separation of variables, the wavefunction is written as

$$\psi_{nlm}(r,\theta,\phi) = R_{nl}(r), \quad Y_{lm}(\theta,\ \phi) = R(r),$$

$$Y_{lm}(\theta,\phi) = \frac{u(r)}{r}, \quad Y_{lm}(\theta,\ \phi),$$

$R_{nl}(r)$ or $R(r)$ is the radial part of the wavefunction and $Y_{lm}(\theta,\ \phi)$ is the spherical harmonics.

The equation for radial part is reduced to the following form

$$\frac{-1}{2\mu}\frac{\partial^2 u}{\partial r^2} + \left[V_2(r) - \frac{e^2}{\epsilon r} + \frac{l(l+1)}{2\mu r^2}\right] u(r) = E_{nlm}u(r). \quad (8)$$

Equation (8) is solved numerically using FDM for calculation of unpurtubed energy and wavefunction. Here n is principal quantum number, l is angular quantum number and m is the azimuthal quantum number. Here, we have considered two different confining potentials for $V_2(r)$ and the solution of the Schrödinger equation with these potentials is divided into two parts which are given below.

2.1. Case-1: W-M excitons in spherical QD in presence of hydrogenic or donor impurites

The potential for a hydrogenic impurity located at the centre of symmetry of spherical QD has the form

$$V_2(r) = \frac{-Z'}{\epsilon r}, \quad (9)$$

where, Z' is whole number ($Z' = 0, 1, 2, \ldots$). We are solving for only three values of $Z' = 0$, 1 and 2.

The Schrödinger equation, so obtained for this case can be reduced to Eq. (8). The equation in presence of spherical confinement cannot be solved analytically for $l \neq 0$ states, but numerically using FDM. However, for large R, ($R \to \infty$), the equation admits an analytical solution, as described in Appendix A which match very well for low lying states with the numerical solution obtained using FDM as the analytic method is a generalized approximation for large R *i.e.* free system.

2.2. CASE-2: Kratzer Potential

The Kratzer potential is defined as follow

$$V_2(r) = V_0\left(\frac{a}{r} - \frac{a^2}{2r^2}\right). \quad (10)$$

Here, V_0 decides the minima of the potential and a known as the potential parameter determines the position where dip/minima of potential occur. As $r \to \pm\infty$, the potential asymptotically to zero. The strength of the potential is adjusted by changing the ratio of a and r.

The analytical solution for Schrödinger equation using this potential is given in Appendix B and they match reasonably with the numerical results obtained using FDM. Once the energy eigenvalues and eigenvectors are found, the effect of magnetic field can be solved by using the diagonalization method, *i.e.*, we expand the wavefunction in terms of expansion coefficients C_n as $\Phi = \sum_n C_n\ \psi_n$ and substitute in the equation s.t.

$$H\Phi = (H_0 + H_1)\Phi = E'_{nlm}\Phi, \quad (11)$$

where $< \psi_m|H_1|\psi_n >$ using Eq. (7) becomes

$$\frac{e^2B^2}{8\mu c^2} < R_{nl}|r^2|R_{n'l'} >< Y_{lm}|\sin^2(\theta)|Y_{l'm'} > + \frac{eB}{2\mu c} < Y_{lm}|L_z|Y_{l'm'} > . \quad (12)$$

The radial and angular matrix elements are evaluated in Eq. (12) numerically. The dressed wave function after perturbation are given by

$$\Phi_i = \sum_{j=1\to n} C_{ij}\psi_j, \quad (13)$$

where C_{ij} defines the coefficients of multiplication.

2.3. Optical properties

The expressions for both linear and third-order non-linear ACs and RICs are calculated using density matrix formulation. These are dependent on susceptibility of medium which is a tensor quantity derived from the DM. Let a periodic laser $\vec{E}(t)$, of angular frequency ω, be incident on the QD. In the frequency domain, the polarization density $\vec{P}(t)$ is related to the electric field by the optical susceptibility $\chi(\omega)$ as

$$P(t) \sim \epsilon_0 \chi^{(1)}(\omega)\vec{E}e^{(\iota\omega t)} + \epsilon_0 \chi^{(3)}(\omega)\vec{E}e^{(\iota\omega t)},$$

where ϵ_0 is the permittivity of the free space, $\chi^{(n)}$ is the nth order susceptibility of the quantum system.

The analytical expressions of linear and third-order non-linear ACs and RICs in terms of non-linear susceptibility are

$$\begin{aligned}
\alpha^{(1)}(\omega) &= \omega\sqrt{\frac{\mu}{\epsilon_r}} Im[\epsilon_0 \chi^{(1)}(\omega)], \\
\alpha^{(3)}(\omega) &= \omega\sqrt{\frac{\mu}{\epsilon_r}} Im[\epsilon_0 \chi^{(3)}(\omega)], \\
\frac{\Delta n^{(1)}(\omega)}{n_r} &= \frac{Re[\chi^{(1)}(\omega)]}{2n_r^2}, \\
\frac{\Delta n^{(3)}(\omega)}{n_r} &= \frac{Re[\chi^{(3)}(\omega)]}{2n_r^2}.
\end{aligned} \tag{14}$$

Here n_r is refractive index of the medium, $\Delta n^{(1)}(\omega)/n_r$ and $\Delta n^{(3)}(\omega)/n_r$ shows the linear and non-linear relative changes in the refractive index of the medium.

After solving for linear and non-linear susceptibility coefficient, the expression for linear and third-order non-linear ACs and RICs are as follow [46,47]

$$\alpha^{(1)}(\omega) = \omega\sqrt{\frac{\mu}{\epsilon_r}} \frac{N|M_{ij}|^2 \hbar\tau_{ij}}{(E_{ji} - \hbar\omega)^2 + (\hbar\tau_{ij})^2}, \tag{15}$$

$$\begin{aligned}
\alpha^{(3)}(\omega) = -\omega\sqrt{\frac{\mu}{\epsilon_r}} \frac{\mu c I N}{2n_r} \frac{|M_{ij}|^2 \hbar\tau_{ij}}{((E_{ji} - \hbar\omega)^2 + (\hbar\tau_{ij})^2)^2} \Bigg[4|M_{ij}|^2 - (M_{jj} - M_{ii})^2 \\
\times \left(\frac{3E_{ji}^2 - 4E_{ji}(\hbar\omega) + \hbar^2(\omega^2 - \tau_{ij}^2)}{E_{ji}^2 + (\hbar\tau_{ij})^2} \right) \Bigg],
\end{aligned} \tag{16}$$

$$\frac{\Delta n^{(1)}(\omega)}{n_r} = \frac{1}{2n_r^2\epsilon_0} \frac{N|M_{ij}|^2 (E_{ji} - \hbar\omega)}{(E_{ji} - \hbar\omega)^2 + (\hbar\tau_{ij})^2}, \tag{17}$$

$$\begin{aligned}
\frac{\Delta n^{(3)}(\omega)}{n_r} = -\frac{\mu c I N}{4n_r^3\epsilon_0} \frac{|M_{ij}|^2}{((E_{ji} - \hbar\omega)^2 + (\hbar\tau_i j)^2)^2} \Bigg[4|M_{ij}|^2 (E_{ji} - \hbar\omega) - (M_{jj} - M_{ii})^2 \\
\times \left(\frac{(E_{ji} - \hbar\omega)[E_{ji}(E_{ji} - \hbar\omega) - (\hbar\tau_{ij})^2]}{E_{ji}^2 + (\hbar\tau_{ij})^2} - \frac{(\hbar\tau_{ij})^2 \times (2E_{ji} - \hbar\omega)}{E_{ji}^2 + (\hbar\tau_{ij})^2} \right) \Bigg],
\end{aligned} \tag{18}$$

where M_{ij} are the dipole transition matrix element between the i^{th} state and the j^{th} state, c is speed of light in free space, $E_{ji} = E_j - E_i$, is the energy difference between two excitonic states, μ is magnetic permeability of medium, τ_{ji} is the relaxation time between two states, ϵ_r denoted the real component of permittivity, N is the number density, and $I = 2\epsilon_0 n_r c|E|^2$ is the intensity of laser field. The total ACs and RICs is

$$\alpha(\omega, I) = \alpha^{(1)}(\omega) + \alpha^{(3)}(\omega, I), \tag{19}$$

$$\frac{\Delta n(\omega, I)}{n_r} = \frac{\Delta n^{(1)}(\omega)}{n_r} + \frac{\Delta n^{(3)}(\omega, I)}{n_r}, \tag{20}$$

3. Results and discussion

We have calculated theoretical results for a three dimensional W-M exciton in a spherical GaAs QD in a static magnetic field with Kratzer potential confinement and have used laser field interaction for calculating the ACs and RICs. For the calculation of different results, we have used following parameters $m_e^* = 0.067m_e$, $m_h^* = 0.09m_e$, where m_e is the free electron mass, the dielectric constant $\epsilon = 12.4$, $R = 200$ Å, $N = 5.0 \times 10^{20}$ m$^{(-3)}$ and $\tau_{ij} = 1.0/0.14$ ps$^{(-1)}$, $V_0 = 228$ meV, $n_r = 3.2$ for our study unless mentioned other values.

TABLE I. Energy eigenvalues for W-M exciton under spherically confined Kratzer potential for different values of magnetic field. We have $R = 200\mathring{A}$. Results are expressed in meV with Kratzer Potential.

nl	$B = 0T$	$B = 2T$	$B = 5T$
1s	-82.10	-76.48	-53.12
1p	-63.61	-59.90	-43.55
1d	-32.15	-26.95	1.19
1f	7.80	13.64	42.41
2s	27.40	33.90	65.84
2p	52.67	56.65	79.05
2d	97.78	102.69	131.26
2f	156.70	161.85	188.70
3s	193.89	200.18	232.05
3p	226.63	230.46	251.44
3d	285.29	289.93	316.36
3f	362.03	366.85	392.04
4s	414.82	420.99	453.60
4p	454.84	458.57	479.24
4d	526.65	531.19	558.50
4f	620.66	625.34	651.80

We have displayed the energies of excitonic levels for 16 states for various magnetic field values in Table I with Kratzer potential confinement.

The confinement potential and size of QD are antagonists to each other and hence result in distinct energy levels with the Kratzer potential confinement. As there is a competition of attractive and repulsive terms in Kratzer potential, we have few bound states in the system. As shown in table, increasing magnetic field, the energy of all levels also increase which is due to the parabolic dependence on the magnetic field.

Table II, shows the variation of energy of different excitonic levels for distinct hydrogenic impurities. The results are found in good agreement with the analytical solution given in Appendix A. The agreement only holds for low-lying states as this is an approximation without any quantum confinement, so even if we have taken a large R value, the angular quantum number (l) still has an impact. We also observe that the number of states matching with analytic results increases with an increase of Z'. This is due to an increase of attractive coulombic interaction due to which the system is getting more bound. It can be noted that coulombic potential has interesting effects on the energy levels of the system.

Using the linearly polarized periodic laser we have studied the optical ACs and RICs for different transitions. Figures 1, 2, 3, and 4 shows the study of the total nonlinear optical properties of the W-M exciton in Kratzer potential at a magnetic field strength of 2 T with and without the confinement in Kratzer potential in which solid curve is for with Kratzer potential confinement and dotted curves is for without Kratzer potential confinement. We have calculated DM elements with and without magnetic fields and also compared their results for various transitions. The intensity of the laser is varied to highlight the non-linear effects.

TABLE II. Energy eigenvalues for W-M exciton for large radius $R = 5000$ Å, $a = 20$ Å at $B = 0$ T. Results are expressed in meV. The numerical results using FDM match well for the low lying states with the analytical results using Appendix A.

nl	$V_2(r) = 0$	$V_2(r) = -1/\epsilon r$	$V_2(r) = -2/\epsilon r$
1s	0.04	-3.40	-13.59
1p	0.08	-0.85	-3.40
1d	0.13	-0.38	-1.51
1f	0.19	-0.20	-0.85
2s	0.16	-0.85	-3.40
2p	0.24	-0.38	-1.51
2d	0.33	-0.19	-0.85
2f	0.43	-0.03	-0.54
3s	0.35	-0.38	-1.51
3p	0.47	-0.17	-0.85
3d	0.60	0.03	-0.54
3f	0.74	0.23	-0.31
4s	0.63	-0.16	-0.85
4p	0.79	0.08	-0.53
4d	0.96	0.34	-0.28
4f	1.14	0.58	0.00

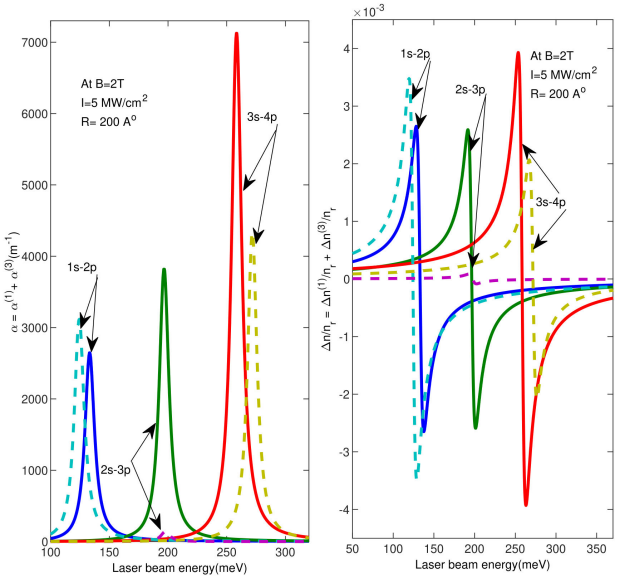

FIGURE 1. Absorption Coefficients and Refractive Index Changes variation with laser beam intensity for the transitions ns-mp in Kratzer potential at $B = 2$ T, with Confinement radius R is taken as 200 Å. Solid lines are with Kratzer potential confinement of exciton in spherical QD and dotted lines are for without potential confinement of exciton in spherical QD.

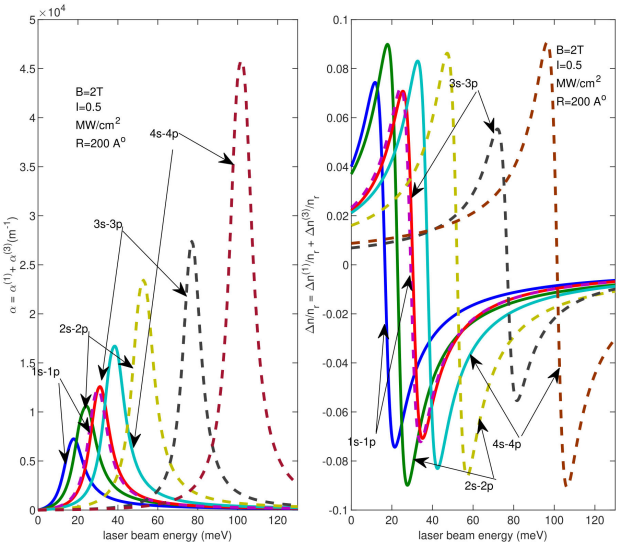

FIGURE 2. Absorption Coefficients and Refractive Index Changes variation with laser beam intensity for the transitions ns-np in Kratzer potential at $B = 2$ T, with Confinement radius R is taken as 200 Å. Solid lines are with Kratzer potential confinement of exciton in spherical QD and dotted lines are for without potential confinement of exciton in spherical QD.

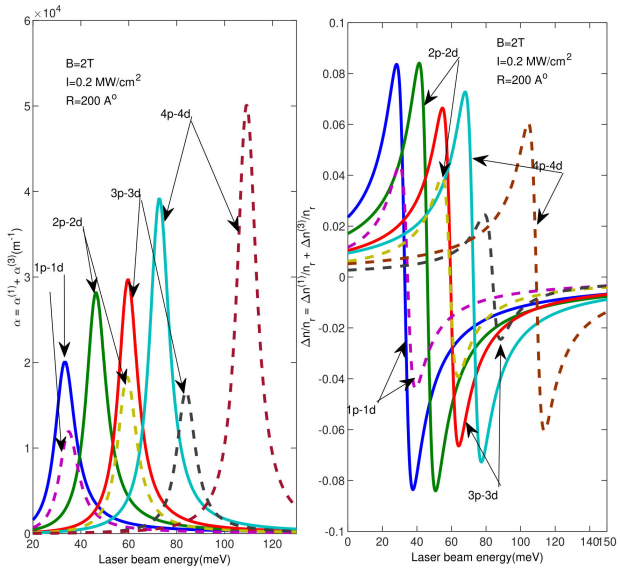

FIGURE 3. Absorption Coefficients and Refractive Index Changes variation with laser beam intensity for the transitions np-nd in Kratzer potential at $B = 2$ T, with Confinement radius R is taken as 200 Å. Solid lines are with Kratzer potential confinement of exciton in spherical QD and dotted lines are for without potential confinement of exciton in spherical QD.

Figure 3 shows the optical ACs and RICs for $ns-(n+1)p$ transitions at $B = 2$ T *i.e.* $1s-2p, 2s-3p, 3s-4p$ with the help of an infrared laser beam of intensity 5 MW/cm^2. Here Solid lines are with Kratzer potential confinement of exciton in spherical QD and dotted lines are for without potential confinement of exciton in spherical QD. It is clear that the $2s-3p$ transition has drastically modified ACs and RICs

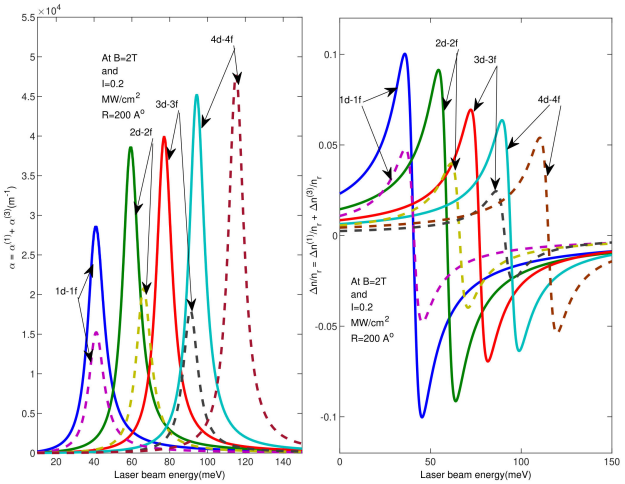

FIGURE 4. Absorption Coefficients and Refractive Index Changes variation with laser beam intensity for the transitions nd-nf in Kratzer potential at $B = 2$ T, with Confinement radius R is taken as 200 Å. Solid lines are with Kratzer potential confinement of exciton in spherical QD and dotted lines are for without potential confinement of exciton in spherical QD.

with Kratzer potential as compared to $1s-2p$ and $3s-4p$ transitions, we see a blueshift in $1s-2p$ transition and $3s-4p$ transition shows a redshift with the Kratzer potential confinement in the presence of the magnetic field. As with the presence of Kratzer potential, we see an interplay with the coulomb and Kratzer term, also the DM element has a significant role, so it is not fixed that in a particular manner we will see redshift or blueshift.

Figure 4 shows the ACs and RICs for $ns-np$ transition *i.e.* $1s-1p$, $2s-2p$, $3s-3p$, $4s-4p$ at $B = 2$ T using infrared laser beam of intensity 0.5 MW/cm^2. Solid lines are with Kratzer potential confinement of exciton in spherical QD and dotted lines are for without potential confinement of exciton in spherical QD.

From Fig. 4, The $ns-np$ excitonic transitions show a decrease in the amplitude of optical AC and RIC peaks with the presence of Kratzer potential for along with a redshift in energy for all the transitions *i.e.* $1s-1p$, $2s-2p$, $3s-3p$, and $4s-4p$ which is expected as resulted from distinct states on using the confinement potential.

Figure 5 represents the ACs and RICs for $np-nd$ excitonic transitions *i.e.* $1p-1d, 2p-2d, 3p-3d, 4p-4d$ with the intensity of laser beam 0.2 MW/cm^2, and Fig. 6 displays the ACs and RICs for $nd-nf$ excitonic transitions *i.e.* $1d-1f$, $2d-2f$, $3d-3f$, $4d-4f$ with the intensity of laser beam 0.2 MW/cm^2 at $B = 2$ T.

The Figs. 5 and 6 shows that with the effect of Kratzer potential confinement, the excitonic optical ACs and RICs transition peaks occur at low laser beam energy(mid infrared range) *i.e.* a redshift is observed from the without Kratzer potential case of $np-nd$ and $nd-nf$ transitions. For $1p-1d$, $2p-2d$, and $3p-3d$ ($1d-1f$, $2d-2f$, and $3d-3f$) excitonic transition peaks amplitude enhances but the amplitude of $4p-4d$ ($4d-4f$) decreases.

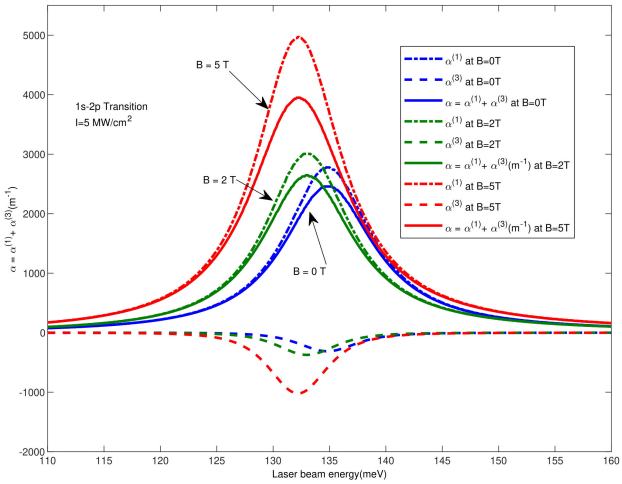

FIGURE 5. Absorption Coefficient variation with the energy of laser beam intensity in the presence of Kratzer potential (a) for $1s-2p$ Transition, with different magnetic field strength.

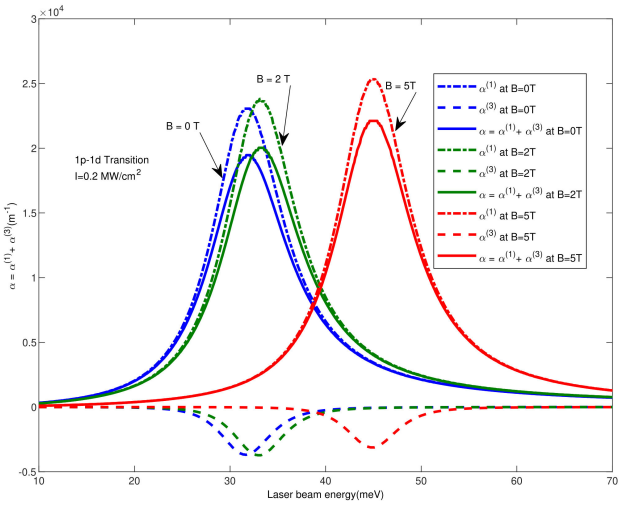

FIGURE 6. Absorption Coefficient variation with the energy of laser beam intensity in the presence of Kratzer potential for $1p-1d$ Transition, with different magnetic field strength.

These results explain that the linear ACs and RICs are independent of intensity changes and nonlinear ACs and RICs vary with change in intensity. It is very interesting to note that the size of QD plays an important role in the optical property for a given transition. For small $R(\leq 100$ Å), it is revealed that Kratzer potential confinement, in general, enhances the optical properties for excitonic transitions but in large $R(\geq 200)$ Å, it is transition dependent.

These results give an insight into which particular excitonic transitions are favorable. We have also found that the DM element need not necessarily increase with an increase in the magnetic field strength, some got decreased *e.g.* For $R = 100$ Å for $1d-1f$ transition with $B = 0$ T, the DM element is 62.4810 atomic units (a.u.) and with $B = 5$ T, it is 59.5641 a.u. Similarly, for $1p-1d$, for $B = 0$ T, DM element is 57.9851 a.u. and with $B = 5$ T, it is 55.3439 a.u. whereas for $1s-1p$ and $1s-2p$ for $B = 0$ T DM element is 54.9043 a.u. and 3.2126 a.u. and for B = 5 T, it is 55.4881a.u. and 6.1203 a.u. respectively.

To elaborate more on the difference of strength of the magnetic field, in Figs. 7 and 8 we have shown ACs for W-M exciton single transition $1s-2p$ and $1p-1d$ in Kratzer potential for different magnetic field strength and intensity 5 MW/cm^2 and 0.2 MW/cm^2 for $R = 200$ Å and $a = 100$ Å respectively.

From Fig. 7, we observe a redshift with an increase in the magnetic field strength which implies lowering of energy gap with increasing strength of magnetic field between $1s$ to $2p$ transition. In Fig. 8 we observe blueshift with an increase in the magnetic field strength. This explains that the interaction of different states with the external magnetic field is dependent on the principal and angular quantum number of different states.

4. Summary and conclusion

In this work, we have used Kratzer potential confinement for the study of electronic levels of Wannier-Mott exciton in spherical confinement in the presence of magnetic field and calculated dipole matrix elements for investigation of linear and non-linear Absorption coefficients and linear and third-order non-linear refractive index changes using a static laser field radiation. From the results, we have found the various factors affecting energy eigenvalues and eigenfunctions including the size of the quantum dot, potential parameter, and magnetic field strength, which gives insight into the controlled energy of exciton levels. The redshift or blueshift in optical ACs and RICs is dependent on the principal quantum number as well as on angular quantum number along with the strength of the magnetic field applied. We also observed that there are few transitions in which the confinement potential increases and in some decreases the amplitude of the excitonic ACs and RICs. This understanding of excitonic transitions is very helpful for designing optoelectronic devices and concludes with the tuning of factors affecting optical properties. This study is an asset for future work in the field of optoelectronic devices.

All the authors contributed equally to the manuscript.

Declaration of interests

The authors declare that they have no known competing financial interests or personal relationships that could have appeared to influence the work reported in this paper.

Appendix A

The Analytical solution for Hydrogenic or donor impurity [48], for 3D, the potential is

$$V(r) = -\frac{Z}{\epsilon r} + \frac{l(l+1)}{r^2} = -\frac{A}{r} + \frac{l(l+1)}{r^2}, \qquad \text{(A.1)}$$

where

$$A = \left(\frac{1}{\epsilon}\right). \tag{A.2}$$

The radial and angular equations are

$$R''_{nl}(r) + \frac{2}{r}R'_{nl}(r) - \frac{l(l+1)}{r^2}R_{nl}(r) + 2\mu\left(E + \frac{A}{r}\right)R_{nl}(r) = 0, \tag{A.3}$$

$$L^2 Y_{lm}(\theta,\phi) - l(l+1)Y_{lm}(\theta,\phi) = 0. \tag{A.4}$$

Using variable transformation

$$\kappa = \sqrt{(-8\mu E)}\ \ r, \quad \rho = \left(\sqrt{\frac{-\mu}{2E}}\right)(A),$$

$$\delta(\delta+1) = l(l+1), \tag{A.5}$$

where for bound states we have $\rho > 0$ and real $\kappa > 0$, and imposing boundary condition on radial equation above, we have

$$R''(\kappa) + \frac{2}{\kappa}R'(\kappa) + \left(\frac{-1}{4} + \frac{\rho}{\kappa} - \frac{\delta(\delta+1)}{\kappa^2}\right)R(\kappa) = 0. \tag{A.6}$$

The solution for the above equation is given as

$$R_{n_r l}(\kappa) = G_{nl}\exp(-\kappa/2)\kappa^{\delta}{}_1F_1(-n_r, 2\delta+2; \kappa), \tag{A.7}$$

where

$$\xi = \frac{2A}{n_r + \delta + 1}, \tag{A.8}$$

and

$$G_{nl} = \left[(\xi)^3\frac{(n_r+2\delta-2)!}{(n_r)!2(n_r+1)}\right]^{(1/2)}, \tag{A.9}$$

which after normalization becomes

$$R_{nl}(r) = \left[\frac{(\xi)^{2\delta+3}(n_r)!}{2(n_r+\delta+2)(n_r+2\delta+1)!}\right]^{(1/2)} \times \exp(-G_{nl}r/2)r^{\delta}L^{2\delta+1}_{n_r}(r), \tag{A.10}$$

and $it's$ energy eigenvalues is

$$E_{nl} = \frac{-2\mu A^2}{[2n_r+2l+2]^2}. \tag{A.11}$$

So, the total wavefunction is given as

$$\psi_{nlm}(r) = G_{nl}R_{nl}(r)Y_{lm}(\theta,\ \phi). \tag{A.12}$$

Appendix B

The Analytical solution for Kratzer potential [48], for 3D, the potential is

$$V(r) = -\frac{(V_0 a + \frac{1}{\epsilon})}{r} + \frac{V_0 a^2}{r^2} + \frac{l(l+1)}{r^2} = -\frac{A}{r} + \frac{B}{r^2} + \frac{l(l+1)}{r^2}, \tag{B.1}$$

where

$$A = \left(V_0 a + \frac{1}{\epsilon}\right) \quad \text{and} \quad B = V_0 a^2. \tag{B.2}$$

The radial and angular equations are

$$R''_{nl}(r) + \frac{2}{r}R'_{nl}(r) - \frac{l(l+1)}{r^2}R_{nl}(r) + 2\mu\left(E + \frac{A}{r} - \frac{B}{r^2}\right)R_{nl}(r) = 0, \tag{B.3}$$

$$L^2 Y_{lm}(\theta,\phi) - l(l+1)Y_{lm}(\theta,\phi) = 0. \tag{B.4}$$

Using variable transformation

$$\kappa = \sqrt{(-8\mu E)}r, \quad \rho = \left(\sqrt{\frac{-\mu}{2E}}\right)(A),$$

$$\delta(\delta+1) = 2\mu B + l(l+1), \tag{B.5}$$

where for bound states we have $\rho > 0$ and real $\kappa > 0$, and imposing boundary condition on radial equation above, we have

$$R''(\kappa) + \frac{2}{\kappa}R'(\kappa) + \left[\frac{-1}{4} + \frac{\rho}{\kappa} - \frac{\delta(\delta+1)}{\kappa^2}\right]R(\kappa) = 0. \tag{B.6}$$

The solution for the above equation is given as

$$R_{n_r l}(\kappa) = G_{nl}\exp(-\kappa/2)\kappa^{\delta}{}_1F_1(-n_r, 2\delta+2; \kappa), \tag{B.7}$$

where

$$\xi = \frac{2A}{n_r + \delta + 1}, \tag{B.8}$$

and

$$G_{nl} = \left[(\xi)^3\frac{(n_r+2\delta-2)!}{(n_r)!2(n_r+1)}\right]^{(1/2)}, \tag{B.9}$$

which after normalization becomes

$$R_{nl}(r) = \left[\frac{(\xi)^{2\delta+3}(n_r)!}{2(n_r+\delta+2)(n_r+2\delta+1)!}\right]^{(1/2)} \times \exp(-G_{nl}r/2)r^{\delta}L^{2\delta+1}_{n_r}(r), \tag{B.10}$$

and $it's$ energy eigenvalues is

$$E_{nl} = \frac{-2\mu A^2}{[2n_r+1+\sqrt{((2l+1)^2)+8\mu B}]^2}. \tag{B.11}$$

So, the total wavefunction is given as

$$\psi_{nlm}(r) = G_{nl}R_{nl}(r)Y_{lm}(\theta,\ \phi). \tag{B.12}$$

1. W. Yao, Z. Yu, Y. Liu, B. Jia, Linear and nonlinear optical absorption coefficients and refractive index changes in strained GaN/AlN quantum dots, Phys. E Low-Dimensional Syst. *Nanostructures*. **41** (2009) 1382. https://doi.org/10.1016/j.physe.2009.03.003.
2. E. Feddi, A. Talbi, M.E. Mora-Ramos, M. El Haouari, F. Dujardin, C.A. Duque, Linear and nonlinear magneto-optical properties of an off-center single dopant in a spherical core/shell quantum dot, *Phys. B Condens. Matter.* **524** (2017) 64. https://doi.org/10.1016/j.physb.2017.08.057.
3. A.D. Yoffe, Advances in Physics Semiconductor quantum dots and related systems: Electronic, optical, luminescence and related properties of low dimensional systems, *Adv. Phys.* **50** (2001) 1. https://doi.org/10.1080/00018730010006608.
4. G. T. Einevoll, Confinement of excitons in quantum dots, *Phys. Rev. B*, **45**, (1992) 7. https://doi.org/10.1103/PhysRevB.45.3410.
5. T. Chakraborty, Nanoscopic quantum rings: a new perspective, in Advance in Solid State Physics, edited by B. Kramer (Springer, Berlin, Heidelberg, 2003), Vol. 43, pp. 79-94 , https://doi.org/10.1007/978-3-540-44838-9$_6$.
6. B. Çakir, Y. Yakar, A. Özmen, M.Ö. Sezer, M. Sahin, Linear and nonlinear optical absorption coefficients and binding energy of a spherical quantum dot, *Superlattices Microstruct.* **47** (2010) 556. https://doi.org/10.1016/j.spmi.2009.12.002.
7. I. Karabulut, Ü. Atav, H. Safak, M. Tomak, Linear and nonlinear intersubband optical absorptions in an asymmetric rectangular quantum well, Eur. Phys. J. B. **55** (2007) 283. https://doi.org/10.1140/epjb/e2007-00055-1.
8. K. L. Jahan, A. Boda and A. Chatterjee, Ground state energy of an exciton in a spherical quantum dot in the presence of an external magnetic field, *AIP Conf. Proc.* **1661** (2015) 080008. https://doi.org/10.1063/1.4915399.
9. J. Flórez, and A. Camacho, Excitonic effects on the second-order nonlinear optical properties of semi-spherical quantum dots, *Nanoscale Res. Lett.* **6** (2011) 1. https://doi.org/10.1186/1556-276X-6-268.
10. V. Prasad, P. Silotia, Effect of laser radiation on optical properties of disk shaped quantum dot in magnetic fields, *Phys. Lett. Sect. A Gen. At. Solid State Phys.* **375** (2011) 3910. https://doi.org/10.1016/j.physleta.2011.09.010.
11. L. Shi, Z.W. Yan, Optical properties of an exciton trapped by an ionized donor in ellipsoidal quantum dots under electric field and hydrostatic pressure, *Int. J. Mod. Phys. B.* **33** (2019) 1. https://doi.org/10.1142/S021797921950108X.
12. G. Grosso and G. P. Parravicini, Chapter 1 - Electrons in One-Dimensional Periodic Potentials, Solid State Physics (Elsevier Science, Amsterdam, 2000), http://dx.doi.org/10.1016/B978-0-12-385030-0.00001-3.
13. A.L. Roest, J.J. Kelly, D. Vanmaekelbergh, E.A. Meulenkamp, Staircase in the Electron Mobility of a ZnO Quantum Dot Assembly due to Shell Filling, *Phys. Rev. Lett.* **89** (2002) 1. https://doi.org/10.1103/PhysRevLett.89.036801.
14. A. Cao, Z. Liu, S. Chu, M. Wu, Z. Ye, Z. Cai, Y. Chang, S. Wang, Q. Gong, Y. Liu, A facile one-step method to produce craphene-CdS quantum dot nanocomposites as promising optoelectronic materials, *Adv. Mater.* **22** (2010) 103. https://doi.org/10.1002/adma.200901920.
15. L. Dallali, S. Jaziri, J. El Haskouri, P. Amorós, Optical properties of exciton confinement in spherical ZnO quantum dots embedded in SiO2 matrix, *Superlattices Microstruct.* **46** (2009) 9076. https://doi.org/10.1016/j.spmi.2009.10.009.
16. L. Lu, W. Xie, Z. Shu, Combined effects of hydrostatic pressure and temperature on nonlinear properties of an exciton in a spherical quantum dot under the applied electric field, *Phys. B Condens. Matter.* **406** (2011) 3735. https://doi.org/10.1016/j.physb.2011.06.081.
17. I. Karabulut, S. Baskoutas, Linear and nonlinear optical absorption coefficients and refractive index changes in spherical quantum dots: Effects of impurities, electric field, size, and optical intensity, *J. Appl. Phys.* **103** (2008) 1. https://doi.org/10.1063/1.2904860.
18. G. Safarpour, A. Zamani, M.A. Izadi, H. Ganjipour, Laser radiation effect on the optical properties of a spherical quantum dot confined in a cylindrical nanowire, *J. Lumin.* **147** (2014) 295. https://doi.org/10.1016/j.jlumin.2013.11.053.
19. B. Akbarnavaz Farkoush, G. Safarpour, A. Zamani, Linear and nonlinear optical absorption coefficients and refractive index changes of a spherical quantum dot placed at the center of a cylindrical nano-wire: Effects of hydrostatic pressure and temperature, *Superlattices Microstruct.* **59** (2013) 66. https://doi.org/10.1016/j.spmi.2013.03.024.
20. K.L. Jahan, A. Boda, I. V. Shankar, C.N. Raju, A. Chatterjee, Magnetic field effect on the energy levels of an exciton in a GaAs quantum dot: Application for excitonic lasers, *Sci. Rep.* **8** (2018) 1. https://doi.org/10.1038/s41598-018-23348-9.
21. M. Boero, J. M. Rorison, G. Duggan, and J. C. Inkson, A detailed theory of excitons in quantum dots, *Surf. Sci.* **377-379** (1997) 371-375. https://doi.org/10.1016/S0039-6028(96)01420-3.
22. A. O. Govorov, A. V. Kalameitsev, R. Warburton, K. Karrai, S. E. Ulloa, Excitons in quantum-ring structures in a magnetic field: Optical properties and persistent currents, *Phys. E Low-Dimensional Syst. Nanostructures.* **13** (2002) 297. https://doi.org/10.1016/S1386-9477(01)00542-2.
23. W. Que, Excitons in quantum dots with parabolic confinement, *Phys. Rev. B.* **45** (1992) 11036. https://doi.org/10.1103/PhysRevB.45.11036.
24. B. Çakir, Y. Yakar, A. Özmen, Linear and nonlinear optical absorption coefficients of two-electron spherical quantum dot with parabolic potential, *Phys. B Condens. Matter.* **458** (2015) 138. https://doi.org/10.1016/j.physb.2014.11.026.

25. A. Galiautdinov, Ground state of an exciton in a three-dimensional parabolic quantum dot: Convergent perturbative calculation, *Phys. Lett. Sect. A Gen. At. Solid State Phys.* **382** (2018) 72. https://doi.org/10.1016/j.physleta.2017.11.001.
26. R. Khordad, Use of modified Gaussian potential to study an exciton in a spherical quantum dot, *Superlattices Microstruct.* **54** (2013) 7. https://doi.org/10.1016/j.spmi.2012.10.014.
27. M. Molski, J. Konarski, Modified Kratzer-Fues Formula for Rotation-Vibration Energy of Diatomic Molecules, *Acta Phys. Pol. A.* **82** (1992) 927. https://doi.org/10.12693/aphyspola.82.927.
28. C. Berkdemir, A. Berkdemir, J. Han, Bound state solutions of the Schrödinger equation for modified Kratzer's molecular potential, Chem. Phys. Lett. **417** (2006) 326. https://doi.org/10.1016/j.cplett.2005.10.039.
29. S.A. Najafizade, H. Hassanabadi, S. Zarrinkamar, Nonrelativistic Shannon information entropy for Kratzer potential, *Chinese Phys. B.* **25** (2016) 040301. https://doi.org/10.1088/1674-1056/25/4/040301.
30. L. Fortunato, A. Vitturi, New analytic solutions of the collective Bohr Hamiltonian for a β-soft, β-soft axial rotor, *J. Phys. G. Nucl. Part. Phys.* **30** (2004) 627. https://doi.org/10.1088/0954-3899/30/5/006.
31. E.D. Filho, R.M. Ricotta, Morse potential energy spectra through the variational method and supersymmetry, *Phys. Lett. Sect. A Gen. At. Solid State Phys.* **269** (2000) 269. https://doi.org/10.1016/S0375-9601(00)00267-X.
32. E. Castro, J.L. Paz, P. Martín, Analytical approximations to the eigenvalues of the Morse potential with centrifugal terms, *J. Mol. Struct. THEOCHEM.* **769** (2006) 15. https://doi.org/10.1016/j.theochem.2005.11.034.
33. F. Ungan, J.C. Martínez-Orozco, R.L. Restrepo, M.E. Mora-Ramos, The nonlinear optical properties of GaAs-based quantum wells with Kratzer-Fues confining potential: Role of applied static fields and non-resonant laser radiation, *Optik (Stuttg).* **185** (2019) 881. https://doi.org/10.1016/j.ijleo.2019.03.129.
34. D.A. Baghdasaryan, E.S. Hakobyan, D.B. Hayrapetyan, H.A. Sarkisyan, E.M. Kazaryan, Nonlinear Optical Properties of Cylindrical Quantum Dot with Kratzer Confining Potential, *J. Contemp. Phys.* **54** (2019) 46. https://doi.org/10.3103/S1068337219010067.
35. K. Batra, V. Prasad, Spherical quantum dot in Kratzer confining potential: study of linear and nonlinear optical absorption coefficients and refractive index changes, *Eur. Phys. J. B.* **91** (2018) 298. https://doi.org/10.1140/epjb/e2018-90432-x.
36. M. Heddar, M. Moumni, M. Falek, Non-Relativistic and Relativistic Equations for the Kratzer Potential plus a Dipole in 2D Systems, ArXiv. (2019).
37. A. Dehyar, G. Rezaei, A. Zamani, Electronic structure of a spherical quantum dot: Effects of the Kratzer potential, hydrogenic impurity, external electric and magnetic fields, *Phys. E Low-Dimensional Syst. Nanostructures.* **84** (2016) 175. https://doi.org/10.1016/j.physe.2016.05.038.
38. Varsha, P. Silotia, V. Prasad, Study of optical properties of Wannier-Mott exciton in spherical quantum dot in Kratzer potential, *3Rd Int. Conf. Condens. Matter Appl. Phys.* **2220** (2020) 020154. https://doi.org/10.1063/5.0002124.
39. H.F. Kisoglu, Non-relativistic analytical solutions of the Kratzer potential for a perturbed system in a magnetic field, *Eur. Phys. J. Plus.* **134** (2019) 460. https://doi.org/10.1140/epjp/i2019-12970-9.
40. J.L. $Marín$, R. Riera and S A Cruz, Confinement of excitons in spherical quantum dots, *J. Phys.: Condens. Matter* **10**, (1998) 1349. http://iopscience.iop.org/0953-8984/10/6/017.
41. A. Anitha, M. Arulmozhi, Exciton binding energy in a pyramidal quantum dot, *Pramana-J. Phys.* **90** (2018) 1. https://doi.org/10.1007/s12043-018-1548-7.
42. A. F. Nikiforov and V. B. Uvarov, *Special Functions of Mathematical Physics*, Birkhauser, Basel, 1988, http://dx.doi.org/10.1007/978-1-4757-1595-8.
43. J. Pliva, on a Modified Kratzer Potential, *J. Mol. Spectrosc.* **14** (1999) 7.
44. P. Silotia, H. Joshi, V. Prasad, Multiple Quantum Well in static magnetic field and intense laser pulses, *Phys. Lett. Sect. A Gen. At. Solid State Phys.* **378** (2014) 3561. https://doi.org/10.1016/j.physleta.2014.10.007.
45. V. V. Nautiyal, P. Silotia, Second harmonic generation in a disk shaped quantum dot in the presence of spin-orbit interaction, *Phys. Lett. Sect. A Gen. At. Solid State Phys.* **382** (2018) 2061. https://doi.org/10.1016/j.physleta.2018.05.017.
46. M.R.K. Vahdani, G. Rezaei, Linear and nonlinear optical properties of a hydrogenic donor in lens-shaped quantum dots, *Phys. Lett. Sect. A Gen. At. Solid State Phys.* **373** (2009) 3079. https://doi.org/10.1016/j.physleta.2009.06.042.
47. M.R.K. Vahdani, G. Rezaei, Intersubband optical absorption coefficients and refractive index changes in a parabolic cylinder quantum dot, *Phys. Lett. Sect. A Gen. At. Solid State Phys.* **374** (2010) 637. https://doi.org/10.1016/j.physleta.2009.11.038.
48. K.J. Oyewumi, Analytical solutions of the Kratzer-Fues potential in an arbitrary number of dimensions, *Found. Phys. Lett.* **18** (2005) 75. https://doi.org/10.1007/s10702-005-2481-9.